Intermetallics 55 (2014) 56–65

Contents lists available at ScienceDirect

Intermetallics

journal homepage: www.elsevier.com/locate/intermet

Physical properties of the InPd intermetallic catalyst

M. Wencka [a, **], M. Hahne [b], A. Kocjan [c], S. Vrtnik [c], P. Koželj [c], D. Korže [c], Z. Jagličić [d], M. Sorić [e, 1], P. Popčević [e], J. Ivkov [e], A. Smontara [e], P. Gille [b], S. Jurga [f], P. Tomeš [g], S. Paschen [g], A. Ormeci [h], M. Armbrüster [h], Yu. Grin [h], J. Dolinšek [c, *]

[a] Institute of Molecular Physics, Polish Academy of Sciences, Smoluchowskiego 17, 60-179 Poznań, Poland
[b] Ludwig-Maximilians-Universität München, Department of Earth and Environmental Sciences, Crystallography Section, Theresienstraße 41, 80333 München, Germany
[c] J. Stefan Institute and University of Ljubljana, Faculty of Mathematics and Physics, Jamova 39, 1000 Ljubljana, Slovenia
[d] Institute of Mathematics, Physics and Mechanics and University of Ljubljana, Faculty of Civil and Geodetic Engineering, Jamova 2, 1000 Ljubljana, Slovenia
[e] Institute of Physics, Bijenička 46, POB 304, 10001 Zagreb, Croatia
[f] Adam Mickiewicz University, Department of Macromolecular Physics and NanoBioMedical Centre, ul. Umultowska 85, 61-614 Poznań, Poland
[g] Institute of Solid State Physics, Vienna University of Technology, Wiedner Hauptstr. 8-10, 1040 Vienna, Austria
[h] Max-Planck-Institut für Chemische Physik fester Stoffe, Nöthnitzer Str. 40, 01187 Dresden, Germany

ARTICLE INFO

Article history:
Received 2 April 2014
Received in revised form
7 July 2014
Accepted 10 July 2014
Available online

Keywords:
A. Intermetallics
B. Electrical properties
B. Thermal properties
B. Thermoelectric properties
E. Electronic structure, calculation
G. Catalysis

ABSTRACT

The intermetallic phase InPd is a candidate material for the use as a catalyst in the methanol steam reforming process. To study the connection between the catalytic properties of the surface and the structural and electronic properties of the bulk, we have grown single crystals of the InPd phase by the Czochralski method and determined their electronic, thermal, magnetic and hydrogen-absorption properties. By growing crystals from a high-temperature solution, we could crystallize a slightly off-stoichiometric In-rich composition $In_{1.04}Pd_{0.96}$, which contained a significant amount of constitutional defects in the lattice (Pd vacancies on the Pd sublattice) to retain the CsCl-type structure. The strongly inhomogeneously broadened ^{115}In NMR spectrum and the high residual ($T \rightarrow 0$) electrical resistivity confirmed the presence of constitutional defects. Single crystals of InPd do not absorb hydrogen, as requested for a good hydrogenation catalyst material. Calculated electronic density of states (DOS) shows large contribution of Pd(d) states at the Fermi level. Application of the electron localizability indicator reveals ionic and multi-centre In–Pd interactions stabilizing the crystal structure. The electrical and thermal conductivities of InPd show metallic character, whereas the thermoelectric power and the Hall coefficient both show positive sign, revealing that InPd is a predominant hole-type conductor. The calculated electronic DOS at the Fermi energy is in a good agreement with the experimental value determined from the low-temperature specific heat. Magnetic measurements have shown that InPd is a diamagnet. All results are compared to the chemically related intermetallic compound GaPd. The active–site-isolation concept for increased catalytic selectivity is discussed in relation to the InPd and GaPd structures.

1. Introduction

Elemental palladium and palladium-based materials are important catalysts for the selective hydrogenation of alkynes. This chemical reaction is applied, for example, in the industrial polymerization of ethylene to polyethylene to purify the feedstock from acetylene. In order to avoid poisoning of the downstream polymerization catalyst, the acetylene content has to be lowered from around 1% to the low ppm range. Here the requirement for the hydrogenation catalysts is to effectively convert acetylene in a large excess of ethylene to protect the polymerization catalysts and to do this at the highest possible selectivity, while avoiding total hydrogenation of acetylene to maximize the final polyethylene yield. Selectivity and long-term stability are thus of utmost importance in the field of Pd-based semi-hydrogenation catalysts [1,2]. Recent results on pure Pd have revealed that a fresh Pd catalyst is modified under reaction conditions, as a function of the reactant partial

* Corresponding author. Tel.: +386 1 4773 740; fax: +386 1 4773 191.
** Corresponding author. Tel.: +48 061 869 5206; fax: +48 061 868 4524.
E-mail addresses: mwencka@ifmpan.poznan.pl (M. Wencka), jani.dolinsek@ijs.si (J. Dolinšek).
[1] Present address: Faculty of Textile Technology, University of Zagreb, Prilaz baruna Filipovića 28a, HR-10000 Zagreb, Croatia.

http://dx.doi.org/10.1016/j.intermet.2014.07.007
0966-9795/

pressures in the feed, by both the surface deposits and also by incorporation of the sub-surface species [3]. During the reaction, a Pd–X sub-surface phase (X = C, H) is newly formed, which becomes the actual catalyst for hydrogenation and is responsible for a dramatic change in selectivity – an increase in case X = C and a decrease for X = H. The Pd–C sub-surface phase was found to be 2–3 atomic layers thick, providing selective hydrogenation of alkynes, whereas hydrogenation is unselective when proceeding on Pd surfaces without sub-surface C modification.

At the atomistic level, the increased selectivity of the Pd–C phase can be explained by the altered kinetics, which is mainly based on blocking the very active, but unselective, hydridic hydrogen from the surface. Another way to increase the selectivity is to surround the transition metal atoms by atoms of another – inactive – element following the active–site-isolation concept [4]. When Pd atoms are surrounded solely by atoms of another species, they are isolated by spatial separation and the isolated active sites on the surface enable only a reduced number of possible adsorption configurations for the reactants, leading to a narrower range of reaction products and improved selectivity.

Intermetallic compounds M_mPd_n of palladium with M = Ga or In also follow the site-isolation concept [5]. Such compounds can be reproducibly prepared in a controlled manner and possess ordered crystal structures leading to a uniform surrounding of the catalytically active sites, so that the number of neighboring sites and the distances between them are well-defined. By selecting palladium-based intermetallic compounds with a suitable crystal structure, the active sites can be tailored to the needs of the chemical reaction. In many of these compounds, strong covalent bonding between the Pd and the M atoms is present, providing long-term stability of the catalytic material under reaction conditions and avoiding deactivation. Crystal structures of the M_mPd_n compounds are different from crystal structures of the constituent elements. Together with the covalent bonding, this results in a strongly altered electronic structure that is responsible for the adsorption properties, so that catalytic properties of the intermetallic compounds are usually very different from those of the elements forming the compound [6]. Knowing the surface and bulk electronic properties of a given intermetallic compound is thus essential for the understanding of its catalytic properties.

Intermetallic compounds in the Pd–Ga system have been proven to show superior catalytic selectivity and stability over the commercial Pd-based catalysts [5,7–13]. Catalytic properties of GaPd and Ga_7Pd_3 were tested in the semi-hydrogenation of acetylene in a large excess of ethylene and showed high selectivity and superior stability with the time-on-stream as compared to the commercial Pd/Al_2O_3 supported catalyst material [11]. Regarding the site-isolation concept, the GaPd is especially appealing as it realizes an FeSi–type cubic crystal structure in which a given Pd atom possesses no other Pd atom in the first coordination sphere, providing an ideal site-isolation situation [14] (for the Ga_7Pd_3 structure of the cubic Ir_3Ge_7 type there is only one Pd atom in the first coordination sphere [15]). The electronic and other bulk physical properties of GaPd were reported recently [16] and it was also demonstrated that this material does not absorb hydrogen, thus preventing hydride formation that would result in reduced catalytic selectivity and mechanical instability.

Intermetallic compounds of indium and palladium In_mPd_n are candidates to be used as catalysts in the methanol steam reforming (MSR) reaction to produce hydrogen. Catalytic activity of the In–Pd/In_2O_3 supported catalyst in methanol or ethanol steam reforming has already been demonstrated, where good catalytic performance was attributed to the outstanding properties of In_2O_3 and In–Pd intermetallic compounds such as high selectivity towards CO_2, redox activity and pronounced basicity [17–22]. Lorenz et al. studied Pd–In_2O_3 interaction due to hydrogen reduction and its impact on the MSR [21]. They suggested that the easy reduction of In_2O_3 enables the low-temperature formation of intermetallic compounds In_mPd_n, which are responsible for the observed reactivity and selectivity characteristics. A recent study on the MSR reaction over the Pd–In_2O_3 catalysts with different metal loading also attributed high CO_2 selectivity to the In–Pd compounds [18], which form easily in a H_2 reduction environment and show good catalytic property for the H_2 production and low CO selectivity in the MSR. Methanol decomposition to CO and H_2 on the InPd(110) surface has also been studied theoretically by density functional theory (DFT) [23]. Some works also describe the hydrogenation of N–O functional groups employing the intermetallic compound InPd in a supported state [24,25].

In the present work we focus on physical characterization of the indium–palladium InPd intermetallic compound. We have grown bulk material in a single-crystalline form at the composition $In_{52}Pd_{48}$ (in at.%), corresponding to the formula $In_{1.04}Pd_{0.96}$ [26]. Since catalysis proceeds at the surface, single crystals are preferred for fundamental studies because they allow preparation of well-defined and oriented surfaces. We present bulk electronic, thermal and magnetic properties of the $In_{1.04}Pd_{0.96}$, to serve as a reference for future experimental and theoretical work on the catalysis with In–Pd intermetallic compounds. Assessment of structural disorder in the crystalline lattice by ^{115}In NMR spectroscopy and hydrogen absorption properties of the material, when exposed to a hydrogen gas, are presented, too. The results are compared to those previously obtained on GaPd [16], which can be considered as a prototype catalyst system based on the site-isolation concept. Electrical resistivity, magnetic susceptibility and optical properties of $In_{1-x}Pd_{1+x}$ on the Pd-rich side of the phase diagram (Pd content of 50–58 at.%) were investigated before [27].

2. Synthesis and structural considerations

The phase InPd has a primitive cubic crystal structure of the CsCl (B2) type, space group $Pm\bar{3}m$ (no. 221) with the lattice parameter a = 0.325 nm and two atoms in the unit cell (Fig. 1(a)) [28]. According to the binary phase diagram [29] the homogeneity range of this phase spreads from 45 to 58 at.% Pd at ~700 °C. An oriented InPd single crystal was grown by the Czochralski method, and the details of preparation are described elsewhere [26]. The crystal was grown from an In-rich solution in order to reduce the growth temperatures and accordingly also the In losses due to its high vapor pressure in the melt. By crystal growth from a two-phase sub-liquidus region one always obtains a specific composition of the solid phase that is in equilibrium with the liquid at the growth temperature, so that the final composition of the single crystal cannot be arbitrarily chosen. In our case we crystallized a slightly off-stoichiometric In-rich composition, which resulted in crystals that were in large parts phase-pure and showed radial compositional homogeneity in the central part away from the outer rim. For the physical-property measurements, we have cut a smaller rectangular bar of dimensions 7 × 1.7 × 1.5 mm^3 from the homogeneous region of the parent monocrystal, where the edges of the bar were parallel to the cubic axes. The composition of the bar was determined by EPMA to be $In_{52}Pd_{48}$ (in at.%) with the uncertainty of 0.5% for each element. This corresponds to the chemical formula $In_{1.04}Pd_{0.96}$. In the following we shall refer to our sample by its generic formula InPd, keeping in mind that the actual composition was slightly off-stoichiometric.

The off-stoichiometry introduces structural disorder into the InPd crystal lattice. It is known that cubic AB phases (A = Pd, Fe, Ni or Co, B = In, Ga or Al) can retain the CsCl-type structure even for

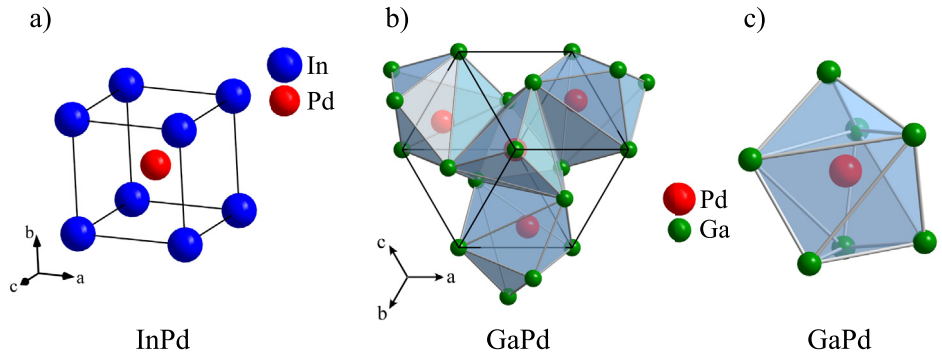

Fig. 1. (a) The cubic unit cell of InPd according to the structural model of Ref. [28]. (b) The cubic unit cell of GaPd according to the structural model of Ref. [14]. (c) Coordination polyhedron formed by seven Ga atoms around a central Pd atom (the first coordination shell of Pd). A similar, but reversed arrangement of seven Pd atoms around the central Ga atom applies also to the first coordination shell of Ga.

strong deviations from stoichiometry by accommodating a large number of constitutional defects into the lattice [30–34]. Within the stability region of the InPd phase, constitutional defects on the In-rich side are vacancies in the Pd sublattice, whereas on the Pd-rich side the deviation from the ideal composition is realized by Pd atoms occupying In positions (anti-site disorder). For a particular In-rich composition $In_{51.5}Pd_{48.5}$, the Pd vacancy concentration on the Pd sublattice was reported to be as high as 6 at.% [32]. Therefore, when growing InPd samples at an off-stoichiometric composition, large concentration of constitutional defects can be expected, which could have a pronounced influence on the physical properties of the material. The site-isolation concept (the In atoms only in the first coordination shell of the Pd atoms) that is expected to result in high catalytic semi-hydrogenation selectivity of the InPd phase would be strictly fulfilled only for the 1:1 stoichiometric composition, whereas in an In-rich off-stoichiometric lattice, the diffusion could move the atoms over the empty sites, so that small direct-bonded Pd clusters might form. In such a case, the site-isolation concept would be fulfilled to a lesser degree.

Contrary to the InPd phase described above, the chemically analogous phase GaPd shows only a very narrow homogeneity range around the 1:1 stoichiometry, so that it can be regarded as a line compound and there are consequently no constitutional defects in the lattice [35]. The GaPd cubic unit cell [14] and the 7-atom Ga coordination polyhedron around a Pd atom are shown in Fig. 1(b and c), respectively. For the GaPd samples of good structural quality (containing no constitutional defects, but other defects like thermal vacancies are still present), the site-isolation concept is thus practically ideally obeyed.

The degree of crystallinity and structural order in the investigated InPd material was estimated in comparison to the GaPd (using the material that was used previously for the determination of physical properties [16]) from the powder XRD spectra shown in Fig. 2. X-ray powder diffraction was performed on a STOE diffractometer equipped with a curved Ge(111) primary monochromator using the Mo $K\alpha_1$ radiation $\lambda = 0.07093$ nm. Powders obtained from single-phase monocrystals by mechanical grinding were annealed under vacuum at 800 °C for 12 h prior to the measurement. The powders were filled-up into 0.3 mm-diameter glass capillaries kept in rotation to obtain texture-free powder diffraction data. The XRD patterns of both compounds consist of sharp diffraction lines typical of materials with good crystallinity and the linewidths are comparable. The difference in the amount of constitutional defects between the InPd and the GaPd cannot be discriminated from the XRD spectra. We shall demonstrate, however, that constitutional defects in the InPd lattice are clearly manifested in the ^{115}In NMR spectrum and the residual electrical resistivity.

3. Results

In the following we present the hydrogen absorption properties, the ^{115}In NMR spectrum, the electronic and thermal transport coefficients (the electrical resistivity, the thermoelectric power, the Hall coefficient and the thermal conductivity), the specific heat and the magnetic susceptibility of the investigated InPd monocrystalline sample. Since the InPd phase symmetry is cubic, no anisotropy of the tensorial physical properties is expected. Electrical and thermal measurements were conducted by a Quantum Design Physical Property Measurement System PPMS 9T (except for the Hall coefficient, which was measured by a laboratory-made apparatus equipped with a 1 T electromagnet), whereas magnetic

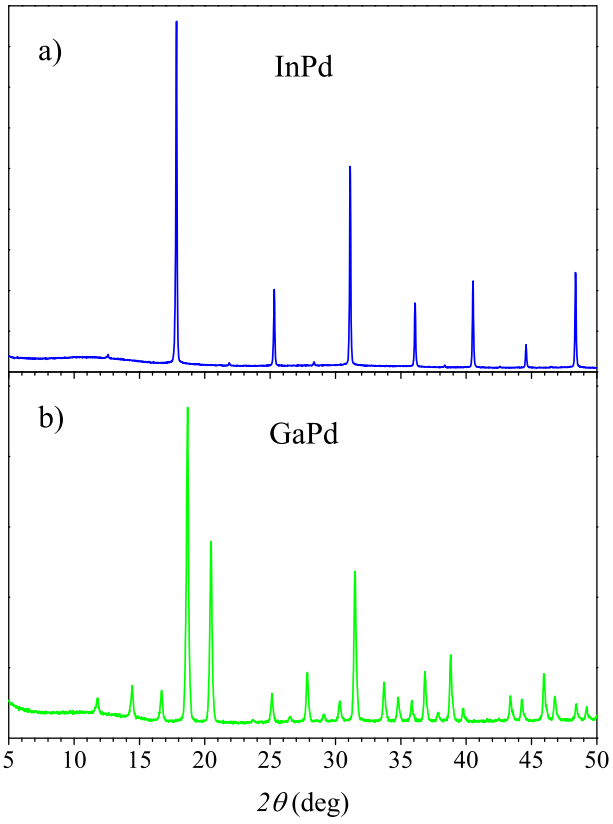

Fig. 2. Powder XRD spectra of (a) InPd and (b) GaPd materials.

measurements were conducted by a Quantum Design MPMS XL-5 SQUID magnetometer equipped with a 5 T magnet.

Electronic structure calculations and analysis of chemical bonding features were accomplished for the ordered stoichiometric (1:1) InPd model using the experimental value of the lattice parameter. The electronic density of states (DOS) was obtained with the WIEN2k program package [36], which is based on the full-potential (linearized) augmented plane-wave ((L)APW) + local orbitals (lo) method. Calculations were performed within the generalized-gradient approximation (GGA) and employing the Perdew-Burke-Ernzerhof (PBE) parametrization of the exchange-correlation potential [37]. The values $R \cdot K_{max} = 10.0$ and $G_{max} = 16.0$ were used and the cut-off energy to separate the core and valence states was −8.0 Ry. A k-point mesh of 200,000 points (58 × 58 × 58) in the full Brillouin zone (4960 in the irreducible Brillouin zone) was used. The atomic sphere radii were set at $r(Pd) = r(In) = 2.45$ bohr.

The electron localizability indicator (ELI, Y) was evaluated in the ELI-D representation [38–40] with an ELI-D module within the TB–LMTO–ASA program package [41]. Topological analysis of the electron density, i.e., estimation of the shapes, volumes and charges of the atoms after Bader (quantum theory of atoms in molecules, QTAIM [42]), and of the electron localizability indicator, e.g., localization of the ELI maxima as fingerprints of the direct atomic interactions, was performed with the program DGrid [43].

3.1. Hydrogen absorption

A selective hydrogenation catalyst should not absorb any hydrogen during the chemical reaction, as the hydride formation involves changes of the structural and electronic properties of the material that directly influence its catalytic performance, resulting in reduced catalytic selectivity and mechanical instability. In order to check for the hydrogen uptake from the gas phase, a bulk piece of InPd single-crystalline material was placed in a 316 stainless-steel Sievert's apparatus, where it was exposed to a hydrogen gas (5.0 grade) of 5 bar pressure at 300 °C for 16 h. Hydrogen uptake was measured thermogravimetrically and by mass spectrometry, by detecting desorbed hydrogen in a heating run. While thermogravimetry (TG) detects mass changes of the hydrided material, mass spectrometry provides information about the distribution of hydrogen desorption temperatures, which are related to the hydrogen bonding energies in the host metallic material. The InPd sample was subjected to a controlled temperature program of a TG-DTA/DSC Gas Analytical System QMS 403 C Aëolos thermal analyzer with an attached mass spectrometer, capable of detecting minute quantities of hydrogen down to 0.005 mass%. The sample was placed in an alumina pot and attached to a thermocouple on the microbalance. After three evacuation/argon refill cycles, the sample was heated from room temperature (RT) to 800 °C with a 20 °C/min heating rate. The upper temperature of the heating run was selected by considering that any stable metal hydride will decompose until 600 °C, so that heating up to 800 °C should be enough to release all the eventually absorbed hydrogen. The mass change of the sample and the hydrogen molecule counts by the mass spectrometer were measured simultaneously. The mass change was found below the detection limit of our measurement system (where the background variations are about 0.005 mass%). No hydrogen release could be noticed also in the H_2 mass spectrum up to the highest temperature (Fig. 3). The vertical axis of the graph shown in Fig. 3 displays the current of ionized H_2 molecules and the measured current value I^{InPd} in the range 10^{-11} A corresponds to the background current, in the absence of any hydrogen release. This demonstrates that InPd did not absorb hydrogen under the employed conditions.

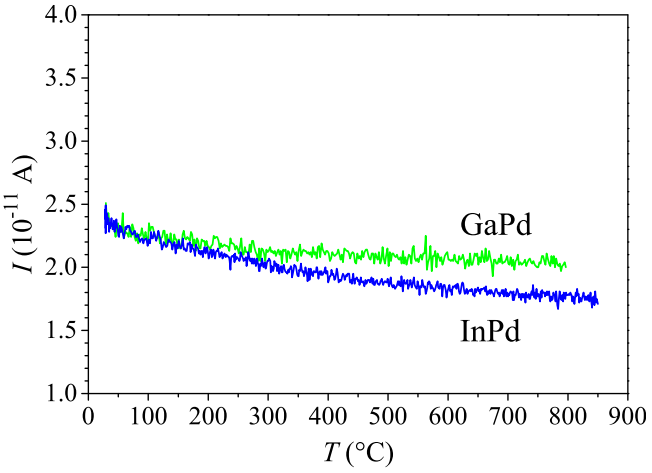

Fig. 3. H_2 mass spectrum of the InPd sample (previously subjected to a pressurized hydrogen gas) upon heating the material from RT up to 800 °C. The corresponding spectrum of GaPd (reproduced from Ref. [16]) is shown as well. The vertical axis displays the current of ionized H_2 molecules. For both materials the current value I in the range 10^{-11} A corresponds to the background current. No hydrogen release can be noticed during heating, indicating no previous hydrogen uptake.

The hydrogen mass spectrum of monocrystalline GaPd (reproduced from Ref. [16]) is also shown in Fig. 3 for comparison. Hydrogenation of GaPd was performed under different conditions, using higher pressure of 55 bar but less clean H_2 atmosphere (4.6 grade), so that comparison to the InPd is only qualitative. The detected current value I^{GaPd} was also in the range 10^{-11} A, again corresponding to the background current in the absence of any hydrogen release. Both InPd and GaPd thus fulfill the requirement of no hydrogen absorption as requested for a selective hydrogenation catalyst.

3.2. Assessment of static disorder in the InPd lattice from ^{115}In NMR spectrum

A convenient way to observe static disorder in the lattice on the local atomic scale is to determine the NMR spectrum of quadrupolar nuclei with spin $I > 1/2$, like ^{115}In ($I = 9/2$) in the case of InPd. The nuclear electric quadrupole moment interacts with the electric field gradient (EFG) tensor produced by the neighboring electric charges (ionic and electronic) at the position of the resonant nucleus. Since the EFG falls with the distance from the charges as $1/r^3$, the electric quadrupole interaction is sensitive to local chemical environments only. When the resonant nucleus is located on a crystallographic site with cubic symmetry, the three diagonal elements V_{ii} ($i = x, y, z$) of the EFG tensor become equal and the EFG tensor becomes a scalar. Since V_{ii}s obey the Laplace equation ($V_{xx} + V_{y\,y} + V_{zz} = 0$), this requires $V_{ii} = 0$ and the electric quadrupolar interaction vanishes. Consequently, the NMR spectrum of ordered lattices where the resonant nuclei occupy crystallographic sites with cubic symmetry consists of one or more sharp lines (with their number being equal to the number of inequivalent sites of the resonant nuclei in the unit cell). Any departure of the local chemical environment from cubic symmetry due to structural and/or chemical (substitutional) disorder will result in nonvanishing electric quadrupole interaction, which introduces inhomogeneous broadening of the NMR spectrum due to random variation of the EFG tensor over the subsequent unit cells. The InPd unit cell contains one In atom occupying a cubic crystallographic site at (0,0,0), so that the ^{115}In NMR spectrum of a structurally ordered InPd monocrystalline sample at a stoichiometric 1:1 composition should

consist of a single sharp line. For non-stoichiometric compositions, the Pd vacancies on the Pd sublattice for In-rich samples and Pd antistructure atoms (Pd atoms on the In sublattice) for Pd-rich samples will distort cubic symmetry of the local chemical environments around the resonant ^{115}In nuclei and introduce inhomogeneous broadening of the NMR spectrum. The width of the ^{115}In NMR spectrum can thus be considered as a measure of structural perfectness of the investigated InPd sample.

The ^{115}In NMR experiment was conducted in a magnetic field $B_0 = 4.7$ T. The InPd monocrystalline sample was placed in a magnetic field at an orientation where one of the cubic axes was parallel to the field. The NMR absorption spectrum was found to be very broad, extending over a frequency interval of about 10 MHz, and was recorded by a frequency-sweep technique. The ^{115}In NMR spectrum at the temperature $T = 80$ K is shown in Fig. 4. The spectrum exhibits a typical structure of a quadrupole-perturbed Zeeman resonance, where the narrow, high-intensity line in the middle of the spectrum corresponds to the second-order quadrupole-perturbed central transition $(1/2 \leftrightarrow -1/2)$ of a spin $I = 9/2$ spectrum, whereas the broad "background" line that extends over about 10 MHz represents overlapping first-order quadrupole-perturbed $\pm1/2 \leftrightarrow \pm3/2$, $\pm3/2 \leftrightarrow \pm5/2$, $\pm5/2 \leftrightarrow \pm7/2$ and $\pm7/2 \leftrightarrow \pm9/2$ satellite transitions. The quadrupolar shape of the spectrum reveals that the electric quadrupole interaction is nonzero due to nonvanishing EFG at the sites of ^{115}In nuclei, demonstrating that the symmetry of the electric charge distribution within the local chemical environments around the In sites is lower than cubic. Intrinsic structural disorder on the InPd lattice (Pd vacancies on the Pd sublattice in the case of our In-rich sample) is predominantly the origin of this broken local symmetry. The continuous nature of the inhomogeneous broadening of the NMR spectrum reveals that structural disorder is realized in many different configurations over the subsequent unit cells. Our investigated InPd monocrystalline sample thus contains structural disorder of intrinsic origin, as expected for an off-stoichiometric In-rich composition.

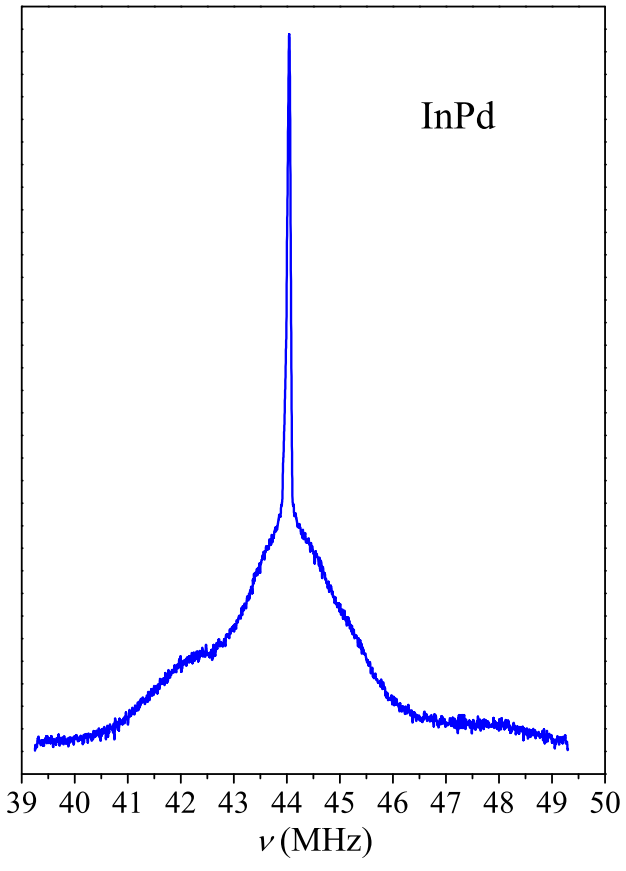

Fig. 4. ^{115}In frequency-swept NMR spectrum of the InPd monocrystal at $T = 80$ K in a magnetic field $B_0 = 4.7$ T.

Comparing the features of the ^{115}In NMR spectrum of InPd to the ^{69}Ga (spin $I = 3/2$) NMR spectrum of GaPd (as reported in Ref. [16]), we note that the ^{69}Ga lines were found narrow (full width at half height of 50 kHz only), showing well resolved central and satellite lines as typical for an ordered lattice. The Ga atoms are not located on cubic sites in the GaPd unit cell, so that the EFG at the position of the ^{69}Ga nuclei is nonzero and the electric quadrupole interaction consequently does not vanish. The orientation-dependence of the ^{69}Ga spectral lines in a magnetic field has enabled the determination of the ^{69}Ga EFG tensor, which was found to possess 3-fold symmetry due to the specific structure of the GaPd unit cell. No spread in the orientation of the EFG tensor's principal axes and eigenvalues was detected, confirming excellent structural order of the GaPd lattice, as expected for a stoichiometric 1:1 compound. The monocrystalline GaPd material can thus be grown to a high structural perfection, whereas our InPd material contains a significant degree of intrinsic structural disorder due to its off-stoichiometric composition.

3.3. Electronic structure and chemical bonding

The theoretical electronic DOS $g(\varepsilon)$ of the stoichiometric 1:1 InPd is shown in Fig. 5(a). Below the Fermi level ε_F, the DOS consists of three well separated regions. The low-energy range ($\varepsilon < -5$ eV) is composed mainly of In(s), Pd(d) and interstitial states. The DOS between -5 and -2 eV is formed mainly by In(p), Pd(d) and interstitial states, with minor admixture of Pd(s). The DOS in the Fermi-level region (shown in the inset on an expanded scale) is formed predominantly by the In(p), Pd(d) and interstitial states. The splitting of the Pd(d) states into three groups reveals their partial participation in the chemical bonding, where the main part remains localized. The electronic DOS of InPd reveals a nonzero density of states at ε_F indicating metal-type behavior in the electronic transport properties. Its value at ε_F amounts to $g(\varepsilon_F) = 0.70$ states/(eV·cell).

The electronic DOS of GaPd was reported before (see Fig. 3 of Ref. [8]), where its subdivision into partial DOSs is also discussed. The DOSs of GaPd and InPd are in general similar to each other with an important difference in the Fermi-level region, which affects their electronic transport properties. To demonstrate this difference, we reproduce in Fig. 5(b) the total DOS of GaPd, with the Fermi-level region shown on an expanded scale in the inset. In the case of GaPd, the DOS variation around ε_F is strong and monotonous and the Fermi energy is pinned to the negative slope of the DOS, so that $(\mathrm{d}g(\varepsilon)/\mathrm{d}\varepsilon)_{\varepsilon_F} < 0$. In the InPd case, ε_F is located just slightly above a local minimum and the variation of the DOS around ε_F is much weaker. The Fermi level is pinned to the positive-slope side of the DOS minimum, so that $(\mathrm{d}g(\varepsilon)/\mathrm{d}\varepsilon)_{\varepsilon_F} > 0$, but the derivative $(\mathrm{d}g(\varepsilon)/\mathrm{d}\varepsilon)_{\varepsilon_F}$ is considerably smaller than the (absolute) derivative in the GaPd case. This point will be discussed in the analysis of the thermoelectric power and the Hall coefficient.

Further insight into the organization of the crystal structure was obtained by applying the analysis of atomic interactions in real space within the electron localizability approach. Integration of the electron density within the atomic basins in accordance with the Quantum Theory of Atoms in Molecules (QTAIM) revealed relevant charge transfer and yielded effective charges of $In^{0.5+}$ and $Pd^{0.5-}$, which are quite similar values to those previously obtained in GaPd [8]. In accordance with the electronegativities of the constituting elements, palladium species carry the negative and the indium

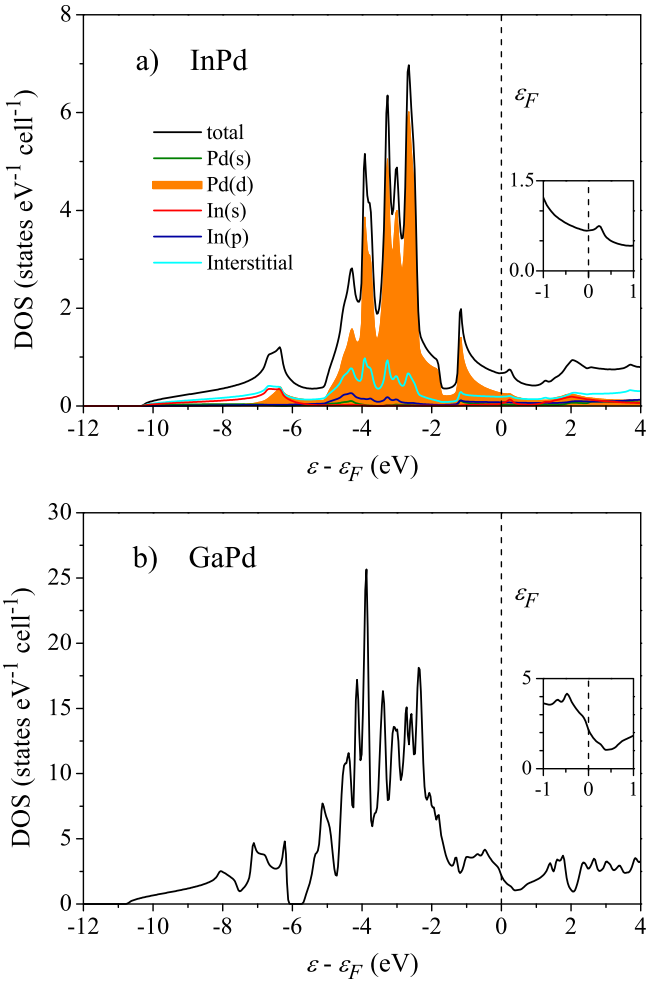

Fig. 5. (a) Calculated total electronic DOS of stoichiometric (1:1) InPd together with the contributions of relevant atomic states. (b) The total DOS of GaPd. The insets show the Fermi-level region on an expanded scale.

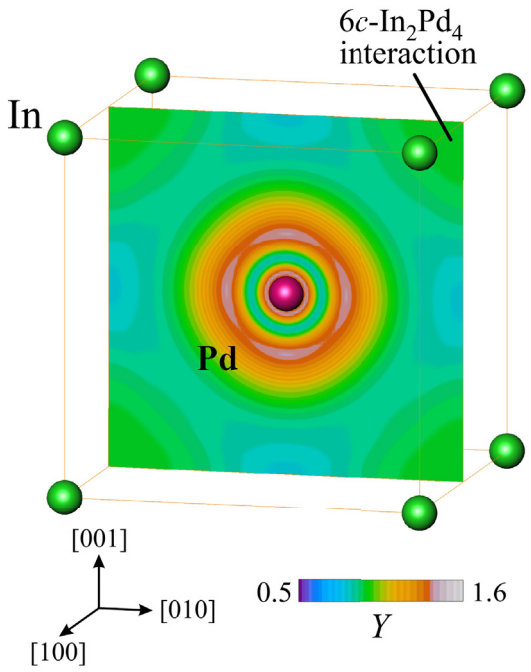

Fig. 6. Chemical bonding in stoichiometric (1:1) InPd: ELI-D distribution (Y) in the (200) plane. 6c-In_2Pd_4 denotes a six-centre interaction between the nearest two indium and four palladium atoms.

atoms the positive charge. The charge transfer represents only a part of atomic interactions which are responsible for the organization of the crystal structure of InPd. The covalent interactions were analyzed by applying the electron localizability indicator ELI-D. Analysis of the distribution of ELI-D in InPd reveals maxima on the line between the In atoms (Fig. 6). Further analysis shows that each bonding basin is in contact with the core basins of two indium and four palladium atomic core basins. As this was already shown for Al_5Co_2 [44], such multi-centre interaction may be considered as a pre-stage of metallic bonding and represents this kind of interactions in the framework of electron localizability approach. The ELI-D distribution in the penultimate shells of palladium deviates from a spherical one (Fig. 6). The structuring of the penultimate shell indicates a participation of these electrons in the bonding within the valence region (cf. DOS above). Combining the QTAIM and ELI-D results leads to the conclusion that the crystal structure of InPd is stabilized by ionic and multi-centre In–Pd interactions.

3.4. Electronic and thermal transport properties

3.4.1. Electrical resistivity

The electrical resistivity $\rho(T)$ of InPd, measured by a standard four-terminal technique in the temperature range between 2 and 350 K, is shown in Fig. 7. Away from the low-temperature saturation limit, the resistivity increases linearly with temperature, where the positive temperature coefficient (PTC) demonstrates predominant role of the electron–phonon inelastic scattering mechanism in the temperature dependence of ρ. The saturation of ρ to a constant plateau in the $T \rightarrow 0$ limit is due to quenched defects in the structure. The resistivity values are metallic, amounting at RT to $\rho_{300K}^{InPd} = 23\ \mu\Omega$cm and the residual resistivity is $\rho_{2K}^{InPd} = 16.6\ \mu\Omega$cm. The relatively high residual resistivity value is a consequence of the intrinsic quenched disorder in the InPd lattice due to its off-stoichiometric composition. For comparison, the RT resistivity of the elemental Pd metal amounts to $\rho_{300K}^{Pd} = 11\ \mu\Omega$cm, which is a factor of 2 smaller than the RT resistivity of InPd.

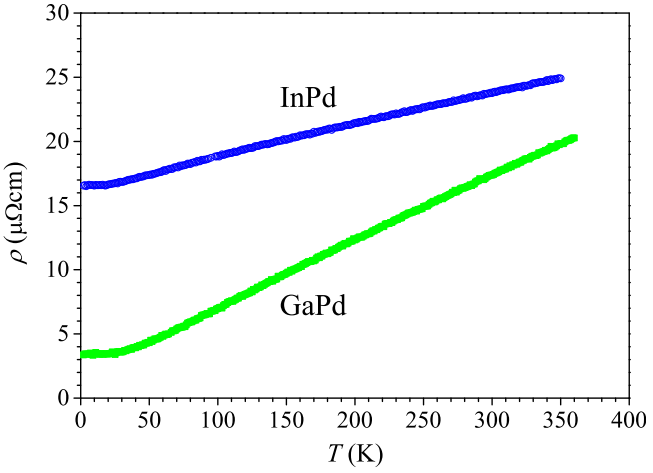

Fig. 7. Temperature-dependent electrical resistivity ρ of InPd. The resistivity of GaPd (reproduced from Ref. [16]) is shown for comparison.

Comparing the InPd resistivity to the resistivity of GaPd [16] (also shown in Fig. 7), the latter also exhibits a PTC with the RT value of $\rho_{300K}^{GaPd} = 18\ \mu\Omega$cm, which is close to the RT resistivity of InPd. The main difference is the residual resistivity, which for the GaPd amounts $\rho_{2K}^{GaPd} = 3\ \mu\Omega$cm, being thus much smaller than the residual resistivity of InPd. The reason for that is much lower density of structural defects in the stoichiometric GaPd. The electrical resistivity results are thus in agreement with a considerably better structural order of the GaPd lattice as compared to InPd.

3.4.2. Thermoelectric power

The thermoelectric power is sensitive to the sign of charge carriers and hence distinguishes between the electrons and holes. The thermopower (the Seebeck coefficient S) of InPd was measured between 2 and 380 K and the result is shown in Fig. 8. The thermopower is small and positive with the RT value amounting to about $S_{300K}^{InPd} = 0.7\ \mu$V/K. For comparison, the thermopower of GaPd (also shown in Fig. 8) is negative, but also relatively small (its RT value amounts to $S_{300K}^{GaPd} = -3.6\ \mu$V/K).

3.4.3. Hall coefficient

The Hall coefficient is another quantity sensitive to the sign of charge carriers and distinguishes between the electrons and holes. The measurements were performed in the temperature interval from 90 to 400 K by a standard ac technique using five-point method in magnetic fields up to 1 T. The experimental error was $\pm 0.1 \times 10^{-10}$ m^{3}C^{-1}. The temperature-dependent Hall coefficient $R_H = E_y/j_x B_z$ of InPd is shown in Fig. 9. R_H^{InPd} is positive and decreases slowly with increasing temperature. The R_H^{InPd} values are in the range 10^{-10} m^{3}C^{-1} (the RT value amounts to $R_{H,300K}^{InPd} \approx 0.7 \times 10^{-10}$ m^3 C^{-1}), which is typical for regular metals and alloys with the charge carrier density of the order 10^{-23} cm^{-3}. The small temperature variation of R_H^{InPd} by less than a factor of two within the investigated temperature interval very likely originates from the temperature-dependent changes of the Fermi surface.

The Hall coefficient of GaPd [16] is shown in Fig. 9 for comparison. R_H^{GaPd} is qualitatively similar to R_H^{InPd} in both magnitude and the type of temperature dependence. The main difference to InPd is the fact that the Hall coefficient and the thermopower of InPd both show positive sign ($R_H^{InPd} > 0$, $S^{InPd} > 0$), whereas they are of opposite signs for GaPd ($R_H^{GaPd} > 0$, $S^{GaPd} < 0$). This result, which is related to the question whether the electrons or holes are the majority charge carriers, will be discussed in the Discussion section.

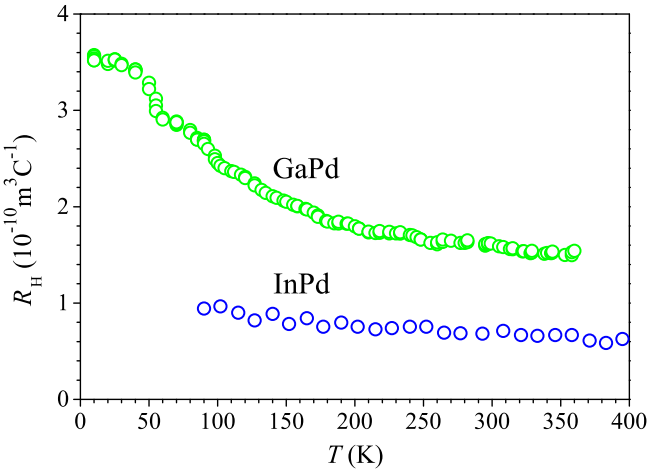

Fig. 9. Temperature-dependent Hall coefficient R_H of InPd. The Hall coefficient of GaPd (reproduced from Ref. [16]) is shown for comparison.

3.4.4. Thermal conductivity

The thermal conductivity κ of InPd is displayed in Fig. 10. κ^{InPd} increases rapidly in the low-temperature region up to about 20 K, whereas at higher temperatures the growth becomes slower and linear. The *RT* value amounts to $\kappa_{300K}^{InPd} = 38$ W/mK. The thermal conductivity of GaPd is also displayed in Fig. 10 for comparison, showing faster low-temperature increase up to about 30 K and then slower growth at higher temperatures with the RT value of $\kappa_{300K}^{InPd} = 50$ W/mK. The reference value for the Pd metal is $\kappa_{300K}^{InPd} = 72$ W/mK, so that both InPd and GaPd can be classified as moderate thermal conductors.

3.5. Specific heat and the electronic density of states at the Fermi energy ε_F

The electronic DOS determines the adsorption properties of any catalytic material. The value of the DOS at the Fermi energy ε_F is conveniently determined from the low-temperature specific heat $C(T)$, which also yields the Debye temperature θ_D of the lattice

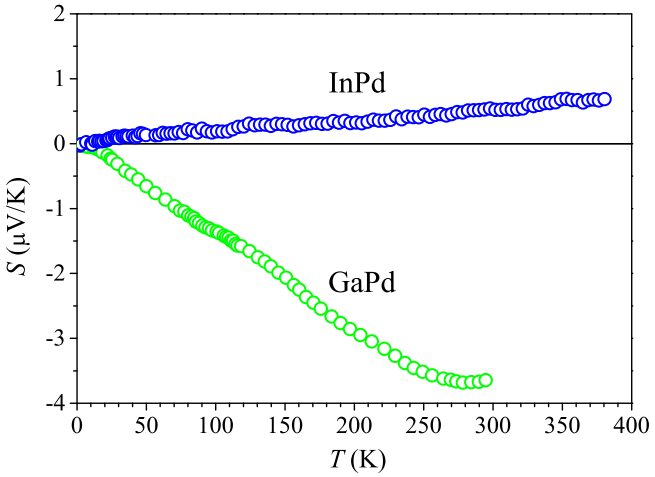

Fig. 8. Temperature-dependent thermoelectric power S of InPd. The thermopower of GaPd (reproduced from Ref. [16]) is shown for comparison.

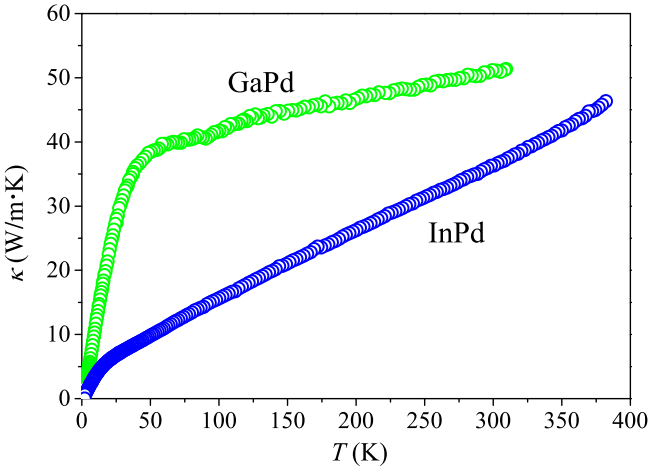

Fig. 10. Temperature-dependent thermal conductivity κ of InPd. The thermal conductivity of GaPd (reproduced from Ref. [16]) is shown for comparison.

vibrations. For nonmagnetic metals and alloys like our InPd (to be verified in the following section on magnetic properties), the specific heat is a sum of the electronic and lattice terms. The electronic specific heat depends linearly on temperature, $C_{el}(T) = \gamma T$, with the electronic specific heat coefficient $\gamma = (\pi^2/3)k_B^2 g(\varepsilon_F)$, where $g(\varepsilon_F)$ is the DOS at ε_F. At low temperatures below about 10 K, the lattice specific heat can usually be well approximated by the Debye model and is expressed as a function of temperature in the form $C_{latt}(T) = \alpha T^3$. The lattice specific heat coefficient α is related to the Debye temperature via the relation $\theta_D = (12\pi^4 R/5\alpha)^{1/3}$, where R is the gas constant. The total specific heat at low temperatures can be written as.

$$C(T) = \gamma T + \alpha T^3. \quad (1)$$

The measurements of the specific heat of InPd were performed in the temperature range between 2 and 300 K. The low-temperature specific heat is displayed in Fig. 11 in a C/T versus T^2 plot, whereas the specific heat in the entire investigated temperature range is displayed in the inset. The analysis of the C/T data with Eq. (1) in the temperature range between 2 and 5 K (solid line in Fig. 11) yielded the experimental values $\gamma^{InPd} = 0.92$ mJ/mol·K^2 and $\theta_D^{InPd} = 243$ K. The reference values of the electronic specific heat coefficient for the constituent metals are $\gamma^{In} = 1.69$ mJ/mol·K^2 and $\gamma^{Pd} = 9.36$ mJ/mol·K^2, so that γ^{InPd} is much closer to γ^{In} than it is to γ^{Pd}.

The electronic specific heat coefficient is a convenient quantity to estimate the deviation of a given metallic system from free-electron-type metals and alloys. For that we compare the experimentally derived electronic specific heat coefficient γ to the corresponding theoretical free-electron value γ_F, calculated from $\gamma_F = 0.136(A/d)^{2/3}(e/a)^{1/3}$ mJ/mol·K^2 [45], where A is the molar mass in g, d the density in g/cm^3 and e/a the number of valence electrons per atom. For our $In_{0.52}Pd_{0.48}$ composition we take $A = 110.8$ g and $d \approx 10.45$ g/cm^3 [33], whereas the ionicity of Pd and In in InPd was estimated before experimentally from magnetic susceptibility data [46] to be about $Pd^{0.6+}$ and $In^{1.0+}$, yielding $e/a = 0.81$. The free-electron value of the electronic specific heat coefficient is then obtained as $\gamma_F^{InPd} = 0.60$ mJ/mol·K^2, yielding the thermal effective mass m^* of the conduction electrons as $m^*/m = \gamma^{InPd}/\gamma_F^{InPd} = 1.53$, where m is the free-electron mass. The departure of m^*/m from unity is of the same order as for free-electron-like metals and alloys, where the mass enhancement originates from the electronic band structure, the coupling of electrons to phonons and the electron–electron interactions.

We are also able to determine the DOS value $g(\varepsilon_F)$ in absolute figures from the equation $\gamma = (\pi^2/3)k_B^2 g(\varepsilon_F) = 2.358\, g(\varepsilon_F)$, where γ is given in units [mJ/mol·K^2] and $g(\varepsilon_F)$ is then obtained in units [states/(eV·atom)]. The experimental value of γ^{InPd} yields $g(\varepsilon_F) = 0.39$ states/(eV·atom). This is to be compared to the theoretical value $g(\varepsilon_F) = 0.70$ states/(eV·cell) (Fig. 5), obtained for the 1:1 stoichiometric InPd. Since there are two atoms in the InPd unit cell, the theoretical value can be recalculated to $g(\varepsilon_F) = 0.35$ states/(eV·atom), giving fair matching to the experimental value obtained for the off-stoichiometric $In_{1.04}Pd_{0.96}$.

Comparing to the GaPd compound [16], we find that its electronic specific heat coefficient $\gamma^{GaPd} = 1.41$ mJ/mol·K^2 is somewhat higher than γ^{InPd} (0.92 mJ/mol·K^2), so that the experimental DOS at ε_F value of GaPd is by a factor $\gamma^{GaPd}/\gamma^{InPd} = 1.53$ larger than the DOS of InPd. The lower DOS at ε_F of InPd is one reason for its larger electrical resistivity (lower electrical conductivity) at elevated temperatures and lower electronic thermal conductivity, as compared to GaPd.

3.6. Magnetic properties

Magnetic susceptibility $\chi = M/H$ was determined in the temperature range 1.9–300 K in the magnetic field $H = 10$ kOe. The susceptibility (Fig. 12(a)) is negative diamagnetic and largely

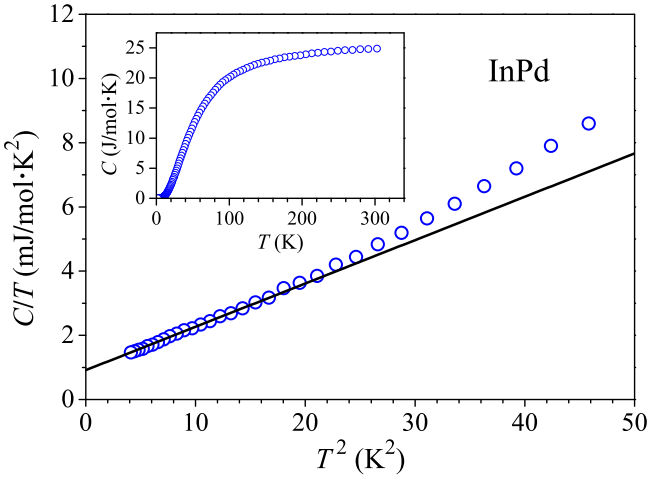

Fig. 11. Low-temperature specific heat of InPd in a C/T versus T^2 plot. Solid line is the fit with Eq. (1). The specific heat in the entire investigated temperature range (2–300 K) is displayed in the inset.

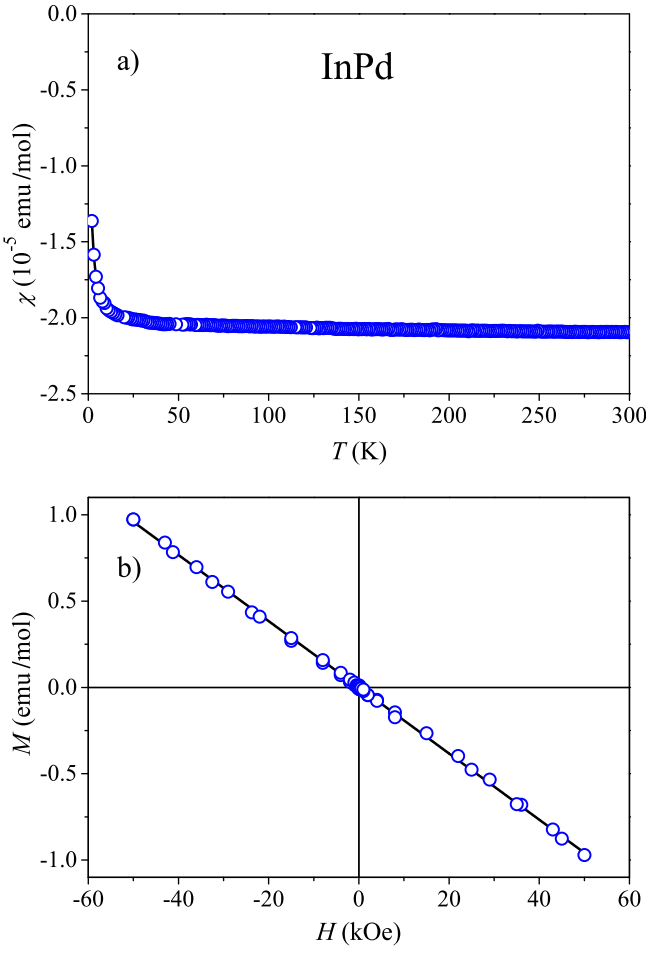

Fig. 12. (a) Temperature-dependent magnetic susceptibility $\chi = M/H$ of InPd in the magnetic field $H = 10$ kOe. (b) Magnetization versus the magnetic field, $M(H)$, at $T = 5$ K.

temperature-independent, except in the low-temperature limit below about 20 K, where a small Curie upturn is observed due to paramagnetic impurities (very likely the residual impurities in the starting materials for the InPd synthesis). The RT susceptibility amounts to $\chi_{300\,K} = -2.1 \times 10^{-5}$ emu/mol. The Larmor diamagnetic core susceptibility of InPd was calculated from literature tables to be in the range $\chi_{dia} = (-2.2, -1.9) \times 10^{-5}$ emu/mol for different possible ionization states of the In and Pd elements, so that χ_{dia} accounts for practically all the experimentally determined susceptibility at RT. This suggests that the two conduction-electron contributions to the susceptibility (the positive Pauli paramagnetic spin susceptibility and the negative Landau orbital diamagnetic susceptibility), which are of the same order of magnitude as χ_{dia}, largely compensate each other.

The magnetization versus the magnetic field, $M(H)$, experiment performed at $T = 5$ K for the magnetic field sweep ±50 kOe is shown in Fig. 12(b). The negative-sloping $M(H)$ straight line confirms the diamagnetic nature of InPd, in agreement with the negative susceptibility χ. InPd is thus a simple diamagnetic intermetallic compound, as can be expected on the basis of magnetic properties of the constituent elements In and Pd. Simple diamagnetism was reported also for the GaPd compound [16].

4. Discussion and conclusions

The InPd intermetallic compound is a candidate material for the use as a catalyst in the methanol steam reforming reaction. Due to its CsCl-type structure, where the atoms of one chemical species are surrounded solely by atoms of the other species in the first coordination shell, the compound is expected to follow the site-isolation concept that assures high catalytic selectivity. In addition, strong In–Pd bonding should provide long-term stability of the compound, which is expected to prevent catalyst deactivation with time under the reaction conditions. Since catalysis proceeds at the surface, well-defined and oriented surfaces prepared from single-crystalline slices are preferred for fundamental studies. For that reason we have grown large single crystals of the InPd phase by the Czochralski method. By performing crystal growth from a high-temperature solution, we could crystallize a specific, slightly off-stoichiometric In-rich composition $In_{52}Pd_{48}$, which yielded crystals that were in large parts phase-pure and showed radial compositional homogeneity in the central part. A consequence of the off-stoichiometry was the introduction of constitutional defects into the lattice (the Pd vacancies on the Pd sublattice), in order that the compound could retain the CsCl-type structure. Since the knowledge of bulk physical properties of the material is important to connect catalytic properties of the surface to the structural and electronic properties of the bulk, we have determined the electronic, thermal, magnetic and hydrogen-absorbing properties of the InPd monocrystal. Throughout the paper the results are compared to the GaPd compound, which can be grown at the 1:1 stoichiometric composition and is considered as a prototype catalyst system that practically ideally obeys the site-isolation concept.

The strongly inhomogeneously broadened ^{115}In quadrupole-perturbed Zeeman NMR spectrum and the relatively high residual $T \to 0$ electrical resistivity confirm the presence of a large concentration of constitutional defects in the InPd lattice at the given off-stoichiometric composition, suggesting that the site-isolation concept could be fulfilled to a lesser extent in the investigated InPd than it is in the GaPd. InPd did not absorb any hydrogen when exposed to a H_2 atmosphere. Comparison to the GaPd shows that both compounds fulfill the requirement of no hydrogen absorption, as requested for a selective hydrogenation catalyst material.

The electronic and thermal transport coefficients of InPd show that the electrical and thermal conductivities are typical metallic and not much lower than the corresponding conductivities of GaPd. The main difference between the two compounds is that InPd shows much higher residual electrical resistivity (the inverse electrical conductivity) $\rho_{T\to 0}$ than GaPd due to the presence of constitutional defects in the lattice. The thermal conductivity of InPd is smaller than that of GaPd for two reasons: (1) the electronic contribution is smaller because of smaller electronic DOS at ε_F in the InPd and (2) the lattice contribution is smaller because the defects in the InPd lattice impede phonon propagation.

The thermoelectric power and the Hall coefficient are both sensitive to the sign of charge carriers and can hence be used to determine whether the investigated compounds are electron- or hole-type conductors. At low temperatures, the temperature dependence of the thermopower can be described by the Mott's expression $S(T) = (\pi^2 k_B^2/3e)(d \ln \sigma(\varepsilon)/d\varepsilon)_{\varepsilon_F} T$, where $\sigma(\varepsilon)$ is the spectral conductivity function. Spectral conductivity is related to the electronic DOS $g(\varepsilon)$ via the Einstein relation $\sigma(\varepsilon) = (e^2/V)g(\varepsilon)D(\varepsilon)$, where $D(\varepsilon)$ is the electronic spectral diffusivity and V is the sample volume. Under the assumption that the energy dependence of the spectral diffusivity can be neglected in the vicinity of the Fermi level, $D(\varepsilon) \approx D(\varepsilon_F)$, $d\ln\sigma(\varepsilon)/d\varepsilon$ can be replaced by $d\ln g(\varepsilon)/d\varepsilon$. The sign of the thermopower is consequently determined by two factors: the sign of the electric charge e and the sign of the DOS derivative at the Fermi energy $(dg(\varepsilon)/d\varepsilon)_{\varepsilon_F}$. We consider first the case of GaPd where the experiments yielded $S^{GaPd} < 0$ and $R_H^{GaPd} > 0$. The theoretical GaPd DOS (Fig. 5(b)) shows that the derivative $dg(\varepsilon)/d\varepsilon$ in the Fermi-level region is negative so that $(dg(\varepsilon)/d\varepsilon)_{\varepsilon_F} < 0$ and the charge carriers must have positive sign (holes) in order that the thermopower is negative. Holes should yield positive Hall coefficient, which is indeed observed in Fig. 9. GaPd is thus a predominant hole-type conductor. For InPd, on the other hand, the thermopower and the Hall coefficient are both positive, $R_H^{InPd} > 0$ and $S^{InPd} > 0$, but their values are considerably smaller than in GaPd. The theoretical InPd DOS (Fig. 5(a)) shows that the derivative $dg(\varepsilon)/d\varepsilon$ at the Fermi-level is positive, $(dg(\varepsilon)/d\varepsilon)_{\varepsilon_F} > 0$, so that the charge carriers must have positive sign (holes) in order that the thermopower is positive. This is again in agreement with the positive Hall coefficient R_H^{InPd}, so that InPd is also a predominant hole-type conductor. The fact that the (absolute) derivative $(dg(\varepsilon)/d\varepsilon)_{\varepsilon_F}$ of InPd is much smaller than the corresponding derivative of GaPd then accounts for the much smaller (absolute) thermopower of InPd, as compared to GaPd.

The experimental electronic DOS at ε_F value of InPd was determined from the low-temperature specific heat, amounting to $g(\varepsilon_F) = 0.39$ states/(eV·atom), which is close to the theoretical value $g(\varepsilon_F) = 0.35$ states/(eV·atom) obtained from first-principles calculations. The value of the electronic specific heat coefficient γ^{InPd} was found to be close to that of pure indium metal, but far from the value of the palladium metal. The departure of γ^{InPd} from the free-electron value by a factor 1.53 is of the same order as for free-electron-like metals and alloys. Comparing to the GaPd compound, we find that the experimental DOS at ε_F value of GaPd is by a factor 1.53 larger than the DOS of InPd (accidentally by the same factor as the ratio of the experimental and theoretical free-electron electronic specific heat coefficients of InPd).

Regarding the magnetic properties, InPd is a simple diamagnetic intermetallic compound and so is GaPd, as can be expected on the basis of nonmagnetic nature of the constituent elements of both compounds.

By considering the InPd and GaPd catalytic performance, the basic question remains to which degree the two compounds obey the site-isolation concept that is of essential importance for the catalytic selectivity in a given chemical reaction. Since more ordered structures lead to more uniform surroundings of the active sites and hence improved selectivity, the well-ordered

stoichiometric 1:1 GaPd seems to be a better example of the site-isolation concept than the investigated InPd, where under the employed growth conditions phase-pure monocrystals could be grown only at an off-stoichiometric In-rich composition, but at the expense of introducing a large concentration of Pd vacancies to retain the CsCl-type structure. Another deficiency comes from the broad existence region of the binary InPd phase in the In–Pd phase diagram, which makes atomic diffusion possible to some extent similar to an alloy, so that long-term stability of the investigated InPd catalyst material may be compromised. Since these problems are absent in PdGa, which is almost a line compound at the stoichiometric 1:1 composition, its catalytic performance is expected to be better as compared to our off-stoichiometric InPd. A future experimental test of the stability and catalytic selectivity of InPd in a realistic chemical reaction should give the answer to this question. It should also be noted that crystal growth at higher temperatures with some tricks to tackle the In vapour pressure might enable to grow InPd from a congruent melt to obtain a more or less stoichiometric compound, where the site-isolation concept would then be fulfilled to a better extent.

Acknowledgments

This work is a result of cooperation within the COST Action CM0904 “Intermetallic compounds as catalysts in methanol steam reforming (IMC-SRM)”. MS, PP, JI, and AS acknowledge support by the Croatian Ministry of Science, Education and Sports, Grant No. 035-0352826-2848. MA acknowledges support by the DFG (AR 617/5-1).

References

[1] See, for a review Borodziński A, Bond GC. Catal Rev Sci Eng 2006;48:91.
[2] Borodziński A, Bond GC. Catal Rev Sci Eng 2008;50:379.
[3] See, for a review Armbrüster M, Behrens M, Cinquini F, Föttinger K, Grin Yu, Haghofer A, et al. ChemCatChem 2012;4:1048.
[4] Sachtler WMH. Catal Rev Sci Eng 1976;14:193.
[5] Armbrüster M, Kovnir K, Grin Yu, Schlögl R. In: Dubois JM, Belin-Ferré E, editors. Complex metallic alloys: fundamentals and applications. Weinheim: Wiley-VCH; 2011. pp. 385–99.
[6] Rosenthal D, Widmer R, Wagner R, Gille P, Armbrüster M, Grin Yu, et al. Langmuir 2012;28:6848.
[7] Armbrüster M, Kovnir K, Behrens M, Teschner D, Grin Yu, Schlögl R. J Am Chem Soc 2010;132:14745.
[8] Kovnir K, Armbrüster M, Teschner D, Venkov TV, Jentoft FC, Knop-Gericke A, et al. Sci Technol Adv Mater 2007;8:420.
[9] Armbrüster M, Schnelle W, Cardoso-Gil R, Grin Yu. Chem Eur J 2010;16:10357.
[10] Osswald J, Giedigkeit R, Jentoft RE, Armbrüster M, Girgsdies F, Kovnir K, et al. Catal 2008;258:210.
[11] Osswald J, Kovnir K, Armbrüster M, Giedigkeit R, Jentoft RE, Wild U, et al. Catal 2008;258:219.
[12] Kovnir K, Teschner D, Armbrüster M, Schnörch P, Hävecher M, Knop-Gericke A, et al. In: BESSY highlights 2007. Berlin: BESSY; 2008. pp. 22–3.
[13] Kovnir K, Osswald J, Armbrüster M, Giedigkeit R, Ressler T, Grin Yu, et al. Stud Surf Sci Catal 2006;162:481.
[14] Armbrüster M, Borrmann H, Wedel M, Prots Yu, Giedigkeit R, Gille P. Z Kristallogr NCS 2010;225:617.
[15] Khalaff K, Schubert K. J Less-Common Met 1974;37:129.
[16] Klanjšek M, Gradišek A, Kocjan A, Bobnar M, Jeglič P, Wencka M, et al. J Phys Condens Matter 2012;24:085703.
[17] Iwasa N, Mayanagi T, Ogawa N, Sakata K, Takezawa N. Catal Lett 1998;54:119.
[18] Men M, Kolb G, Zapf R, O'Connell M, Ziogas A. Appl Catal A 2010;380:15.
[19] Lorenz H, Jochum W, Kötzer B, Sötger-Pollach M, Schwarz S, Pfaller K, et al. Appl Catal A 2008;347:34.
[20] Iwasa N, Takezawa N. Top Catal 2003;22:215.
[21] Lorenz H, Turner S, Lebedev OI, Van Tendeloo G, Klötzer B, Rameshan C, et al. Appl Catal A 2010;374:180.
[22] Umegaki T, Yamada Y, Ueda A, Kuriyama N, Xu Q. Res Lett Phys Chem 2009;2009:631815.
[23] Ye J, Liu C, Ge Q. Phys Chem Chem Phys 2012;14:16660.
[24] Hirano T, Ozawa Y, Sekido T, Ogino T, Miyao T, Naito S. Appl Catal A 2007;320:91.
[25] Krawczyk N, Witonska I, Królak A, Frajtak M, Karski S. Rev Roum Chim 2011;56:595.
[26] Hahne M, Gille P. J Cryst Growth 2014. http://dx.doi.org/10.1016/j.crysgro.2013.11.061.
[27] Galoshina EV, Nomerovannaya LV, Kirillova MM, Shubina TS. Phys Met Metall 1980;50:50.
[28] Hellner E, Laves F. Z Naturforsch A 1947;2:177.
[29] Okamoto H. J Phase Equilib 2003;24:481.
[30] Müller HG, Hahn H. Philos Mag A 1983;50:71.
[31] Balogh AG, Dézsi I, Hahn H, Ghafari M. J Phys F Met Phys 1985;15:1623.
[32] Collins GS, Nieuwenhuis HT. Defect Diffus Forum 2001;194–199:375.
[33] Huang M, Xie F, Yan X, Chang YA. Intermetallics 2001;9:457.
[34] Huang M, Oates WA, Chang YA. Philos Mag 2003;83:589.
[35] Gille P, Ziemer T, Schmidt M, Kovnir K, Burkhardt U, Armbrüster M. Intermetallics 2010;18:1663.
[36] Blaha P, Schwarz K, Madsen GKH, Kvasnicka D, Luitz J. WIEN2k, an augmented plane wave + local orbitals program for calculating crystal properties. Vienna: Techn. Universität; 2001, ISBN 3-9501031-1-2.
[37] Perdew JP, Burke S, Ernzerhof M. Phys Rev Lett 1996;77:3865.
[38] Kohout M. Int J Quantum Chem 2004;97:651.
[39] Wagner FR, Bezugly V, Kohout M, Grin Yu. Chem Eur J 2007;13:5724.
[40] Kohout M. Faraday Discuss 2007;135:43.
[41] Jepsen O, Burkhardt A, Andersen OK. The program TB-LMTO-ASA version 4.7. Stuttgart: Max-Planck-Institut für Festkörperforschung; 1999.
[42] Bader RFW. Atoms in molecules: a quantum theory. Oxford: Clarendon Press; 1994.
[43] Kohout M. DGrid version 4.6; 2011. Radebeul.
[44] Ormeci A, Grin Yu. Isr J Chem 2011;51:1349.
[45] See, e.g. Mizutani U. Introduction to the electron theory of metals. Cambridge: Cambridge University Press; 2001. pp. 39–42
[46] Cho SJ. Phys Stat Sol 1970;41:179.